Effect of Aperture shape on Visibility of Quantum Cryptography System

Adawiya J. Haider
Applied Physics Department,
University of Technology
E-mail:
adawiya_haider@yahoo.com

Azhar I.Hassan
Applied Physics Department,
University of Technology
E-mail:
azhar.hassan@yahoo.com

Ali J. Addie
Applied Physics Department,
University of Technology
E-mail:
alirose12@yahoo.com

Abstract

The main goal in Quantum Cryptography is high security and this can be achieved by using single photon sources, thus we have studied the entangled photon source and how the coincident count rate and visibility could be affected by the optical elements of the system setup.

The present work is a theoretical analysis devoted to investigate the interference pattern of biphoton amplitude generated by spontaneous parametric down conversion (SPDC) in a nonlinear crystal (BBO) pumped by femto-second optical pulses. We have studied the visibility as a function of optical path delay for different parameters, such as the crystal length, aperture diameter, size and shape of the aperture

The shape of interference pattern can be enhanced by using different shapes & sizes of aperture. So in the case of continuous wave (CW)pumping, when using circular aperture the visibility is highest and symmetry shape occurs at lower aperture diameter (b=0.5mm). Asymmetry and wide dip pattern is occurred at larger aperture diameter (b=10mm), when using shifting ring, a negative peak was appeared. In case of pulsed pump asymmetry, patterns occur and increase with increase of crystal length and decreasing aperture diameter. When using slit aperture (vertical and horizontal direction), the coincident count is more symmetric in horizontal with dimension (1x7) mm. All the results of this work are based on several numerical techniques and different programming codes. For example, adaptive Simpson quadrator method have been used to numerically evaluate the double integral in some equations. And adaptive Lobatto quadrator method has been used to numerically evaluate a single integrals. The later method is more efficient when required a high accuracy or a smooth integral.

Keywords: *entangled source; Quantum Cryptography; fs laser**;** quantum optics; quantum information*

1. Introduction

Quantum cryptography (Quantum key distribution) was started from an unusual idea formed in 1969 by graduate student Steven Wiesner[1]. After discussing Wiesner's idea with him, Charles Bennett, a scientist from Bell Labs in New York, continuously thought of his idea over the next few years. This lead to Bennett and another scientist, Gilles Brassard, to come up with quantum cryptography. Once quantum cryptography is used to generate a secure key, the one time pad from classical cryptography, is used to encrypt the message.

The higher security standard in Quantum Cryptography (QC) is insured by entangled photon pairs [2]. A better source allowing maximally entangled forms of all four Bell states was realized in 1995 using a parametric downconversion process with type-II phase matching [3]. In quantum communication, entanglement is used as a source to perform various tasks such as quantum teleportation, dense coding, and quantum cryptography. The latter has become the first commercial application based on full theory of quantum physics, and is currently hunting customers [4,5].

QC begins with the transmission of single or entangled states between Alice and Bob. SPDC, is a non linear optical phenomena, has become one of the most widely used sources for entangled photon. Coincidence count and visibility of these entangled photon have been the most crucial parameter in the QC [6,7].

Quantum-interference patterns generally arise in contexts where only a single parameter, such as polarization, is actively manipulated. However, it has been shown that by making use of all the parameters naturally relevant one can, in fact, modify the interference pattern associated with one parameter such as polarization.

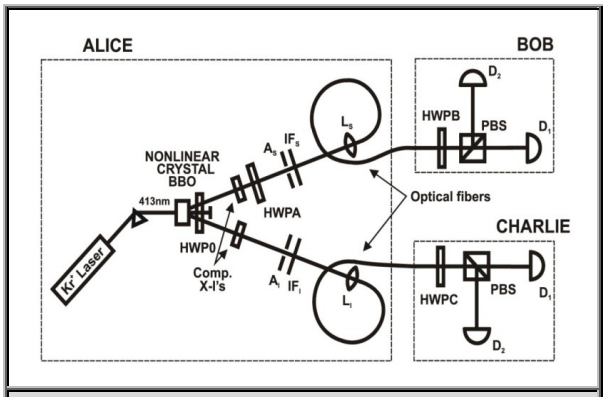

Figure (1) The Proposed Setup. HWP0, HWPA, HWPB, HWPC- half wave plates, Comp. X-Is-compensating crystal, As, Ai- aperture in signal and idler beam, IFs, IFi-interference filters, Ls ,Li-coupling lenses, PBS-polarization beam splitter, D-detectors [14].

One of the most successful ways to analyze quantum cryptography using entangled-photon pair as a source for transmission bits between Alice and Bob is the coincident count rate (quantum interference pattern). When a pump beam incident on a nonlinear crystal , it is affected by different optical elements as shown in Fig (1).The purpose of this letter to demonstrate theoretically how the polarization quantum interference pattern, presented as a function of relative temporal delay between the photons of an entangled pair, is modified by controlling the optical system through different kind of spatial apertures. The effect of the spectral profile of the pump field is investigated by using both a continuous-wave and a pulsed laser to generate SPDC. The role of the spatial profile of the pump field is also studied by restricting the pump-beam diameter at the face of the non linear crystal.

2.1 The Proposal Set-up

The set up under consideration is shown in Fig.(1). In order to realize the full potential of entangled-photon states, it is vital to understand and exploit all those features present in their quantum states from the point of their creation, during their propagation and until their detection.

Generally, the setup can be classified into three parts:

- Generation of two photon states.
- Propagation of these two photon states.
- Detection of the two photon states.

2.2 Generation of Two Photon States

With this motivation a multidimensional analysis of the entangled-photon state generated via SPDC is presented. To admit a broad range of possible experimental schemes consider, three general and fundamentally distinct stages in any experimental apparatus the generation, propagation, and detection of the quantum state are considered.

The work begins with generation by virtue of the weak non linear interaction, we consider the state generated within the first-order time-dependent perturbation theory: [8]

$$\left|\Psi^{2}\right\rangle \sim \frac{i}{\hbar}\int_{t_0}^{t} dt'\, \hat{H}_{\text{int}}(t')\left|0\right\rangle \qquad (1)$$

Here $\hat{H}_{int}(t')$ is the interaction Hamiltonian, (t_o, t) is the duration of the interaction, and $|0\rangle$ is the initial vacuum state.

The interaction Hamiltonian governing these phenomena is: [8,9]

2.THEROTICAL ANALYSIS

$$\hat{H}_{\text{int}}(t') \sim X^{(2)} \int_{v} dr\, \hat{E}_{p}^{(t)}(r,t')\hat{E}_{o}^{(-)}(r,t')\hat{E}_{e}^{(-)}(r,t') + H.c. \qquad (2)$$

Where X(2) is the second-order susceptibility and v is the volume of the nonlinear medium in which the interaction takes place. The symbol Ej(±) (r,t´) represents the positive or(negative) frequency portion of the jth electric field operator with the subscript representing the pump) (p), ordinary (o), and extraordinary (e) waves at position r and time t´, and H.c. stands for Hermitian conjugate.

Due to the high intensity of the pump field we take the coherent-state laser beam to be classical, with an arbitrary spatiotemporal profile given by:[8]

$$E_{p}(r,t) = \int dk_{p}\, \tilde{E}_{p}(k_{p}) e^{ik_{p}.r_{e} - iwp(k_{p})t} \qquad (3)$$

Where Ẽp(Kp) is the complex-amplitude profile of the field as a function of the wave vector kp.

Decomposing the three-dimensional wave vector kp into two-dimensional transverse wave vector qp and frequency wp, so that, eq (3) takes the form:

$$E_p(r,t) = \int dq_p dw_p \tilde{E}_p(q_p; w_p) e^{ik_p z} e^{iq_p \bullet X} e^{-iw_p t} \quad (4)$$

Where X spans the transverse plane perpendicular to the propagation direction z. The ordinary & extraordinary fields can be expressed in terms of the quantum mechanical creation operators â† (q, w) as:[8,10]

$$\hat{E}_j^{(-)}(r,t) = \int dq dw e^{-ik_j z} e^{iq_j \cdot x} e^{iw_j t} \hat{a}_j^{\dagger}(q_j, w_j) \quad (5)$$

Where the subscripts j=o, e

The longitudinal component of k, denoted k, can be written in terms of the (q,w) pair as: [10]

$$\kappa = \left\{ \left[\frac{n_e(w,\theta) w}{c} \right]^2 - |q|^2 \right\}^{\frac{1}{2}} \quad (6)$$

Where Θ is the angle between k and optical axis of the non linear crystal

ne (w, Θ): is the extraordinary index of refraction in the nonlinear medium.

c: is the speed of light in vacuum.

Note that the extraordinary refractive index, ne(w,Θ) in eq. (6) should be replaced by the ordinary refractive index, n0 (w), when calculating for ordinary waves.

Substituting eqs. (4) and (5) into eqs. (1) and (2) yields the wave function of the output of the nonlinear crystal.[8]

$$\left|\Psi^{(2)}\right\rangle \sim \int dq_o dq_e dw_o dw \, \Phi(q_o, q_e; w_o, w_e) \hat{a}_o^{\dagger}(q_o, w_o) \hat{a}_e^{\dagger}(q_e, w_e) |0\rangle \quad (7)$$

with:

$$\Phi(q_o, q_e; w_o, w_e) = \tilde{E}_p(q_o + q_e; w_o + w_e) L \sin c\left(\frac{L\Delta}{2}\right) e^{-i\frac{L\Delta}{2}}, \quad (8)$$

where Δ=kp-ko-ke, where kj(J= p,o,e) is related to the indices (qj,wj) via relations similar to eq. (6). and L is the thickness of the crystal.

2-2-1 Spectral profile of the pump field

In particular there are two cases of the spatial and spectral profile of the pump field that of a poly chromatic plane wave and a monochromatic plane wave. These various cases will be used subsequently for CW and pulse pumped SPDC studies.

First a non–monochromatic plane wave pump field is described mathematically by: [11]

$$\tilde{E}_p(q_p; w_p) = \delta(q_p) \varepsilon_p(w_p - w_p^o) \quad (9)$$

Where $\varepsilon_p(w_p - w_p^o)$ is the spectral profile of the pump field.

Second, a monochromatic plan wave pump field is described by:

$$\tilde{E}_p(q_p; w_p) = \delta(q_p) \delta(w_p - w_p^o) \quad (10)$$

2.3 Propagation of two Photon State

Propagation of the down converted light between the planes of generation and detection is characterized by the classical transfer function of the optical system.

The biphoton probability amplitude at the space-time coordinates (xA, tA) and (xB, tB), where detection will take place, is defined by:[10, 12]

$$A(x_A, x_B; t_A, t_B) = \left\langle 0 \left| \hat{E}_A^{(+)}(x_A, t_A) \hat{E}_B^{(+)}(x_B, t_B) \right| \Psi^{(2)} \right\rangle \quad (11)$$

The explicit forms of the quantum field present at the detection location are represented by:

$$\hat{E}_A^{(+)}(x_A,t_A) = \int dq\,dw\, e^{-iwt_A}\left[H_{Ae}(x_A,q;w)\,\hat{a}_e(q,w) + H_{Ao}(x_A,q,w)\,\hat{a}_o(q,w)\right] \quad (12)$$

$$\hat{E}_B^{(+)}(x_B,t_B) = \int dq\,dw\, e^{-iwt_B}\left[H_{Be}(x_{Be},q;w)\,\hat{a}_e(q,w) + H(x_{Bo},q;w)\,\hat{a}_o(q,w)\right] \quad (13)$$

Where the transfer function Hij (i=A,B and j=e, o) describes the propagation of a (q, w) mode from the nonlinear crystal output plane to the detection plane. Substituting eqs. (7) and (13) into eq. (11) yields a general form for the biphoton probability amplitude [8]:

$$A(x_A,x_B;t_A,t_B) = \int dq_o\,dq_e\,dw_o\,dw_e\,\Phi(q_o,q_e;w_o,w_e) \times\left[H_{Ae}(x_A,q_e;w_e)H_B(xb,qa,wo)\exp\{-i(w_e t_A + w_o t_B)\} + H_{Ao}(x_A,q_o;w_o)H_{Be}(x_B,q_e;w_e)\exp\{-i(w_o t_A + w_e t_B)\}\right] \quad (14)$$

Almost all quantum-interference experiments performed to up date have a common feature, namely that the transfer function Hij in eq. (14), with i= A, B and j=o, e, can be separated in to diffraction-dependent and -independent terms as: [8]

$$H_{ij}(x_i,q;w) = T_{ij}\,H(x_i,q;w) \quad (15)$$

Where the diffraction-dependent terms are grouped in Hij and the diffraction- independent terms are grouped in Tij as shown in Fig (2). Free space, aperture, and, lenses, for example, can be treated as diffraction-dependent element, while beam splitter, temporal delays, and wave plates can be considered as diffraction- independent elements.

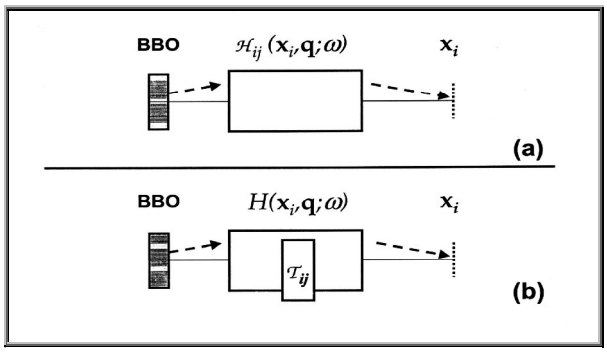

Figure (2) (a) Illustration of the idealized setup for observation of quantum interference using SPDC, (b) Transfer function can be factorized into diffraction dependent and independent component [10].

For collinear SPDC configurations, for example, in the presence of relative optical-path delay (□ between the ordinary and the extraordinary polarized photons, as illustrated in Fig (3) a , Tij is simply:

$$T_{ij} = (e_i - e_j)e^{-iwT\delta_{ej}} \quad (16)$$

Where the symbol δej is the kronecker delta with □ ee=1 and □ eo=0. The unit vector ei described the orientation of each polarization analyzer in the experimental apparatus, while ej is the unit vector that describes the polarization of each down-converted photon.

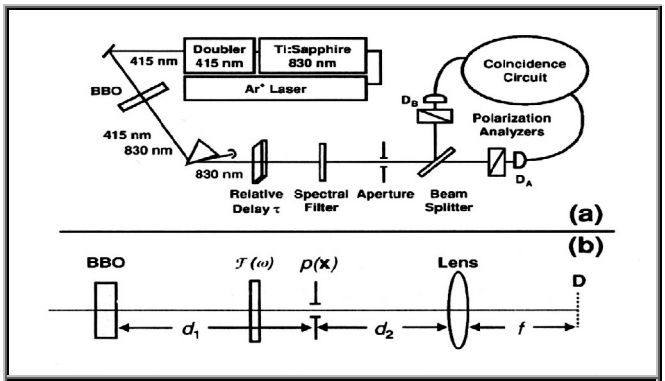

Figure (3) (a) Schematic of the experimental setup for observation of quantum interference using type-II collinear SPDC. (b) The path from the crystal output plane to the detector input plane. F(ω) represents an (optional) filter transmission function, p(x) is an aperture function, and f is the focal length of the lens.[10]

Using the expression for Hij given in eq. (15) in the general biphoton probability amplitude given in eq.

(14), we construct a compact expression for all systems that can be separated into diffraction-dependent and independent element as:[8,10]

$$A(x_A, x_B, t_A, t_B) = \int dq_o dq_e dw_o dw_e \, \phi(q_o, q_e; w_o, w_e) \times \left[T_{Ae} H(x_A, q_e; w_e) T_{Bo} H(x_B, q_o; w_o) e^{-i(w_e t_A + w_o t_B)} + T_{Ao} H(xA, qo; wo) T_{Be} H(xB, qe; we) e^{-i(w_o t_A + w_e t_B)} \right] \quad (17)$$

Eq.(17) given the general form of the biphoton probability amplitude for a separable system.

$$A(x_A, x_B; t_A, t_B) = \int dq_o dq_e dw_o dw_e \tilde{E}_p(q_o + q_e; w_o + w_e) \, L \sin c\left(\frac{L\Delta}{2}\right) e^{-i\frac{L\Delta}{2}} e^{-iweT} x \left[H(x_A, q_e; w_e) H(x_B, q_o; w_o) e^{-i(_w e t_A + w_o t_B)} - H(x_A, q_o; w_o) H(x_B, q_e; w_e) e^{-i(w_o t_A + w_e t_B)} \right] \quad (18)$$

Referring to Fig (3-b), the overall propagation through this system is broken in to free- space propagation from the non linear- crystal output surface (x, 0) to the plane of the aperture (x, d1), free-space propagation from the aperture p1 and to thin lens (x, d1+d2), and finally free-space propagation from the lens to the plane of deflection (Xi, d1 +d2+f), with i=A, B, and d1, d2, & f (focal length of the lens) are indicated.

2.4 Detection of Two Photon State

The formulation of the detection process depends on the scheme to be used. Slow detectors, for example, impart temporal integration, while finite area detectors impart spatial integration.

One extreme case is realized when the temporal response of a point detector is spread negligibly with respect to the characteristic time scale of SPDC, namely the inverse of down-conversion bandwidth.

In this limit the coincidence rate reduces to: [10,13]

$$R = \left| A(x_A, x_B); t_A, t_B) \right|^2 \quad (19)$$

On the other hand, quantum-interference experiments make use of slow bucket detectors. Under these conditions, the coincidence count rate R is readily expressed in terms of the biphoton probability amplitude as:

$$R = \int dx_A dx_B dt_A dt_B \left| A(x_A, x_B; t_A, t_B) \right|^2 \quad (20)$$

Substitution of eq. (18) intoeq. (20) gives an expression for the coincidence count rate given an arbitrary pump profile and optical system.

However, this expansion is widely used for purposes of predicting interference pattern except in certain cases where integration can be swiftly performed.

Continuing the analysis in the Fresnel approximation and the approximation that the SPDC fields are quasi- monochromatic, we can derive an analytical form for the coincidence count rate defined in eq. (20): [6, 10]

$$R(T) = R_o \left[1 - V(\tau) \right] \quad (21)$$

Where Ro is the coincidence rate outside the region of quantum interference. In the absence of spectral filtering

$$V(\tau) = \Lambda\left(\frac{2\tau}{LD} - 1\right) \sin c \left[\frac{wp^o L_2 M_2}{4cd_1} \frac{\tau}{LD} \Lambda\left(\frac{2\tau}{LD} - 1\right) \right] \tilde{P}_A\left(\frac{wp^o LM}{4cd_1} . \frac{2\tau}{LD} e_2\right) \times \tilde{P}_B\left(\frac{wp^o LM}{4cd_1} \frac{2\tau}{LD} e_2\right) \quad (22)$$

where D = (1/uo)-(1/ue) with uj denoting the group velocity for the j-polarized photon. (j =o, e), $M = \partial \ln ne(\frac{\omega^{o}_{p}}{2\theta OA})/\partial \theta e$ and $\Lambda(x) = 1 - |x|$ for $-1 \le x \le 1$ and are otherwise.

The function $\tilde{P}_i$ (with i=A, B) is the normalized Fourier transform of the squared magnitude of the aperture function $\tilde{P}_i(x)$.

The profile at the function $\tilde{P}_i$ within eq.(22) plays a key role in the results presented in this work. Λ determines the shape of the quantum interference pattern, resulting in a symmetric triangular die. The function (sinc(x)) in eq. (22) is approximately equal to unity for all practical experimental configurations and therefore plays a insignificant role in calculations of V(□).

When SPDC is generated using a finite-bandwidth pulsed pump field, eq. (22) becomes. [10]

$$V(\tau) = \Lambda\left(\frac{2\tau}{LD} - 1\right) v_p(\tau)\ \tilde{P}_A\left(\frac{wp^{o}LM}{4cd_1}\frac{2\tau}{LD}e_2\right)\tilde{P}_B\left(\frac{wp^{o}LM}{4cd_1}.\frac{2\tau}{LD}e_2\right) \quad (23)$$

Where the function $\{\sin c\left[\frac{wp^{o}L_2M_2}{4cd_1}\frac{\tau}{LD}\Lambda\left(\frac{2\tau}{LD}-1\right)\right]\}$ in eq. (22) is simply replaced by □p, which is the deviation of the angular pump frequency, and all other parameters are identical to those in eq. (22). The visibility of the dip in this case is governed by the band width of the pump field. It is clear from eq.(22) that V(τ) can be altered dramatically by carefully selecting the aperture diameter.

2.5 Aperture Characterization

Now studying the effect of the aperture shape, size, and its location via the function $\tilde{P}_i(q)$, on polarization quantum- interference pattern [10].

1- Quantum interference with circular aperture:

The mathematical representation of the intensity distribution throw this kind of aperture is given in terms of the Bessel function J1,

$$\tilde{P}_i(q) = 2\frac{J_1(b|q|)}{b|q|} \quad (24)$$

Where, b is circular aperture diameter

2. Quantum interference with slit apertures:

Considering the use of a vertical slit to investigate the transverse symmetry of the generated photon pair, and ˜P(q) takes the explicit form

$$\tilde{P}(q) = \frac{\sin\ (be_1.q)}{be_1.q}\frac{\sin\ (ae_2.q)}{ae_2.q} \quad (25)$$

Where, a and b are the dimensions of slit (a= 7 mm, b= 1 mm)

3. Quantum interference with increased acceptance angle.

To increase the limited acceptance angle of detection system by reducing the distance between the crystal and aperture plane and using the set up in Fig.(3 a)by replaceing the position of one aperture with two apertures, one is put in front of each detector .

4. Pump field diameter effect with assumption that pump field is plane wave.

5. Shifted-Aperture effect.

Here we must include one additional factor in eq.(23):

$$\cos\left[\frac{w_p\ LM}{4cd_1}\frac{2t}{LD}e\ .(S_A - S_B)\right] \quad (26)$$

a) Quantum interference with shifted- slit apertures.

b) Quantum interference with shifted- ring (annular apertures). The function in this case yield

$$\tilde{P}_A\frac{2}{b-a}\left[\frac{J_1(b|q|)}{|q|} - \frac{J_1(a|q|)}{|q|}\right] \quad (27)$$

The solution of equations used were achieved by MATLAB language. (Version 7.4). The Steps followed to solve eq. (21) considered other eqs. (24), (25), (26) & (27) for different crystal thickness and aperture diameter with different aperture shapes and sizes.

The effect of both the aperture shape and size, via the function P(q), will have significant effect on the polarization quantum-interference patterns. Such an aperture can be described by the Bessel function J1.In this work we use =351 for a CW laser pump, and pulsed pump wavelength= 415nm.

3. Results and Discussion

The observed normalized coincidence rates correspond to the sort of quantum-interference pattern is displayed in Fig. (4), as a relative optical-path delay is varied, for various values of aperture diameter (b=1~10mm) placed 1 m from the crystal. The observed interference pattern, calculated by eq. (23 & 24), is seen to be more strongly asymmetric for larger values of 1 b. As the aperture becomes wider, the phase-matching condition between the pump and the generated down-conversion allows a greater range of (q; w) modes to be admitted. Those (q; w) modes that overlap less introduce more distinguishability and reduce the visibility of the quantum-interference pattern and introduce an asymmetric shape.

The theoretical plots of the visibility quantum – interference pattern of the full compensation delay =LD/2, as due to the crystal thickness, is plotted in Fig (5). For various aperture diameters placed at 1m from this crystal, full visibility is expected only in the limit of extremely thin crystals, or with the use of an extremely small aperture diameter.

If the pump field is pulsed, then there are additional limitations on the visibility that emerge as a result of the broad spectral band width of the pump field. . Fig (6) shows visibility plot similar to Fig (5) for the pulsed-pump case, while in pulsed pumping at the same crystal thickness and aperture diameter the visibility is less than in CW pumping.

The absorbed normalized coincidence rates from a pump of 415nm pulses and a aperture placed 1m from the crystal, along with the expected theoretical curves, assuming a Gaussian spectral profile for the pump, are displayed in Fig (7) as function of relation optical –path delay for 2.5 mm, 5mm, and 10mm aperture diameter.

The asymmetry of the interference pattern that increasing crystal thickness is even more visible in the pulsed regime. Fig (7) shows the symmetry increases with reducing aperture diameter, and the visibility reduces with increasing crystal thickness Circular apertures are used after the down-conversion crystal in the majority of quantum-interference experiments involving relative optical-path delay. However, by again departing from convention, one can also use a vertical slit aperture to investigate the effect of and exploit transverse symmetry of the generated photon pairs. The dataCW -pumped 1.5-mm BBO. Noting that the optical axis of the crystal falls along the vertical axis, these results verify that the dominant portion of distinguishability lies along the optical axis. The orthogonal axis (horizontal here) provides a negligible contribution to distinguishability, so that virtually full visibility is achievable, despite the wide aperture along the horizontal axis. The most dramatic effect observed is the symmetrization of the quantum-interference pattern and the recovery of the high visibility, despite the wide aperture along the horizontal axis.

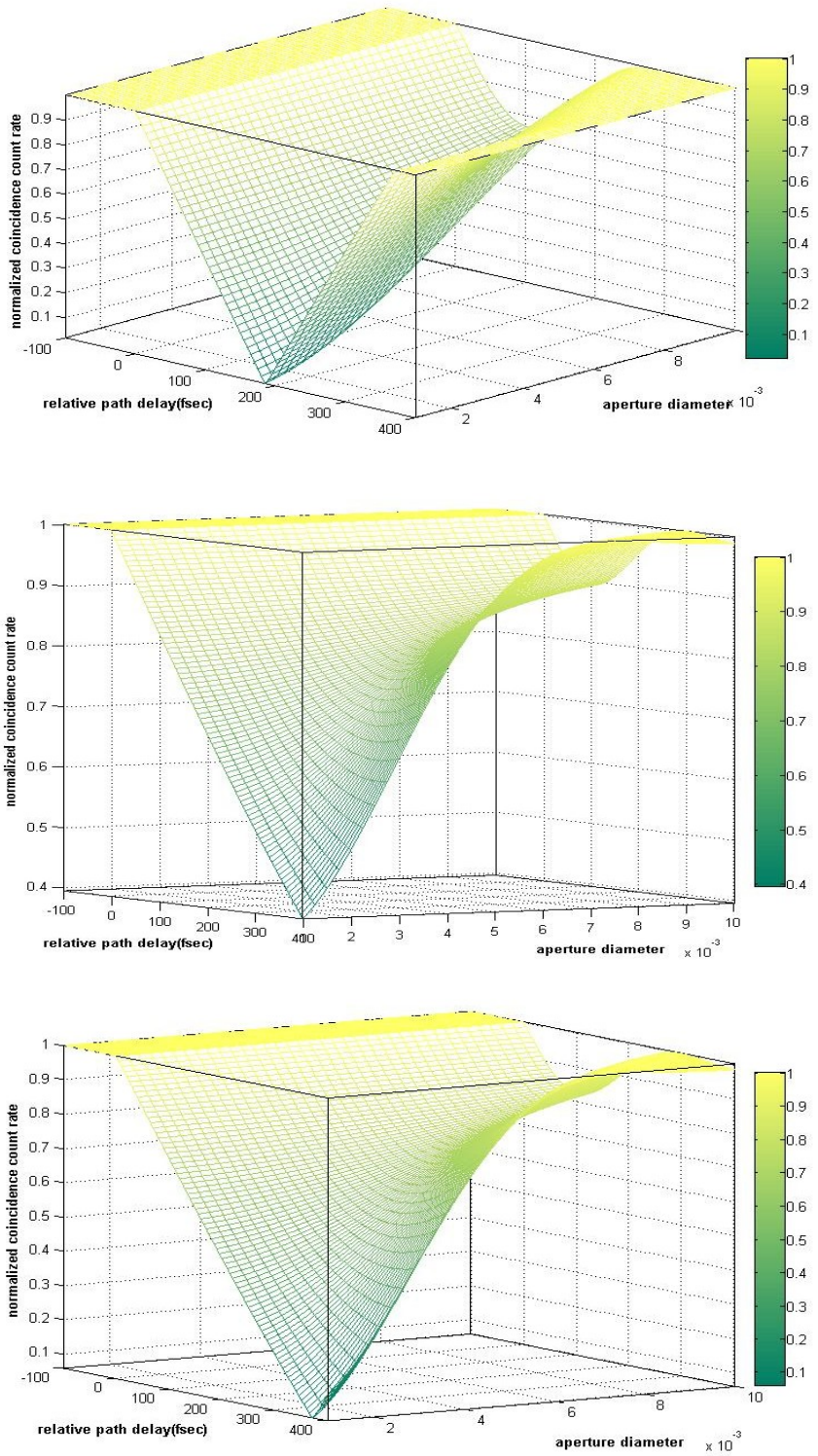

Figure (4) Coincident count rate as a function of optical path delay for different aperture diameter (b).for various crystal length(a- L=1.5, b- L=3, c- L= 5mm).

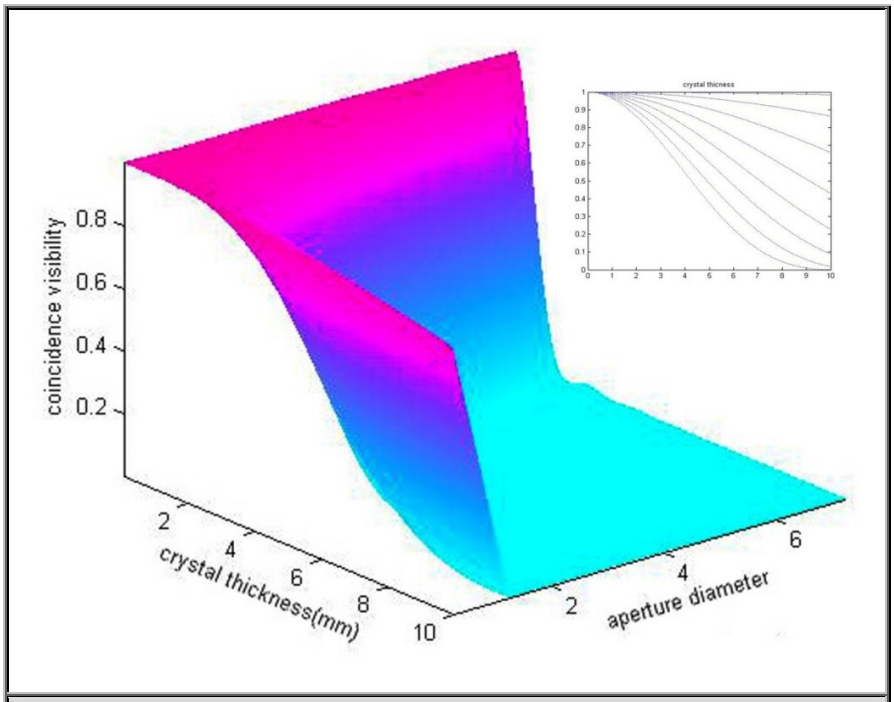

Figure (5) Coincident visibility as a function of crystal thickness for different circular aperture diameter for CW SPDC.

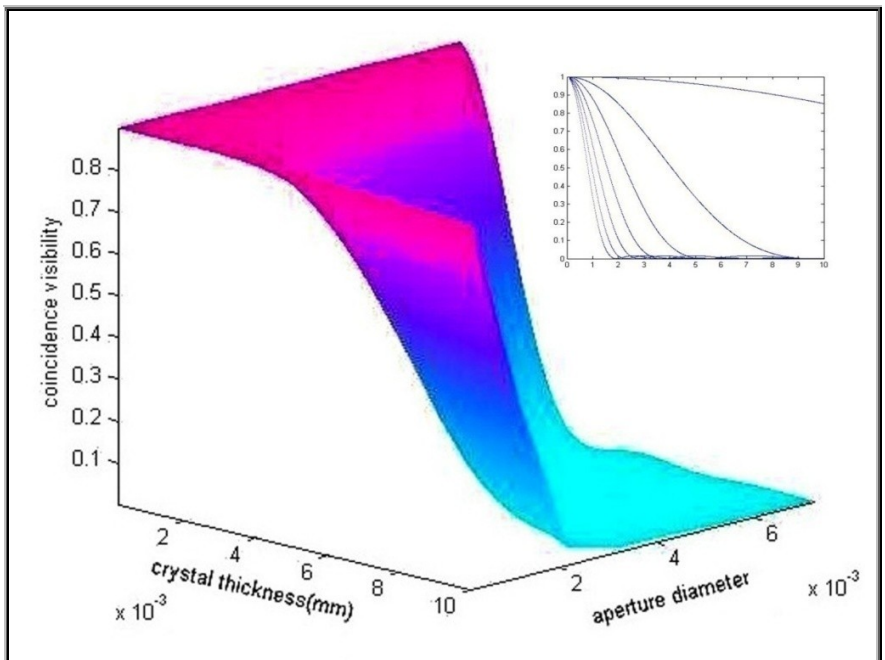

Figure (6) coincident visibility as a function of crystal thickness for various circular aperture diameter for pulsed SPDC.

A practical benefit of such a slit aperture is that the count rate can be increased dramatically by limiting the range of transverse wave- vectors along the optical axis of the crystal, inducing indistinguishability and allowing a wider range along the orthogonal axis to increase the collection

efficiency. A high count rate is required for many applications of entangled photon pairs. Researchers have generally suggested complex means of generating high-flux photon pairs, but we see that intelligent state engineering provides an elegant solution.

The quantum interference pattern is highly asymmetric and has low visibility when using the vertical slit. And indeed is similar to that obtained using a wide circular aperture (as shown in Fig. (4)). The solid curve is the theoretical quantum - interference pattern expected for the vertical slit aperture used.

In complementary experiment has also been performed using a horizontal slit the parameter a and b in eq. (25) are interchanged so that a=1mm and b=7mm. a CW-pumped 1.5mm BBO in the presence of this aperture. The most dramatic effect absorbed is the summarization pattern and the recovery of the high visibility, despite the wide aperture along the horizontal –axis.

Fig (9) shows that the lowest and most asymmetric pattern occurred when the vertical slit a aperture was +450. This verifies that the effect of axis selection is solely due to the spatiotemporal distribution of SPDC and not related to any birefringence or dispersion effects associated with the linear elements.

The effective acceptance angle is increased by reducing the distance between the crystal and the aperture plane. Fig (10) displays the quantum interference patters (normalized coincidence rates) from a CW- pumped 1.5 mm BBO Crystal as a faction of relative optical path delay for various values of the aperture diameter b placed 750mm from the crystal, for data on the curve with lamest visibility. The limiting apertures in the system were determined by the dimensions of the polarization analyzers, which measure 7mm across.

To demonstrate the independence of the interference pattern on the beam size of the pump, using a variety of a perfumes at the front surface of the crystal. Fig (11) shows the normalized coincidence rate from a CW-pumped 1.5mm BBO crystal as a function of relative optical-path a delay for various value of pump beam diameter. This behavior of the interference pattern suggests that the dependence of the quantum interference pattern on the diameter of the pump pulse is negligible.

Fig (12) shows the quantum interference with shifted silt aperture. The curve (a) corresponds to the use of 1×7mm horizontal slit, while anther curve (b) represents the same aperture rotated at (90°) to form vertical slit.

Note that the horizontal slit gives a high visibility interference pattern and the vertical slit gives an asymmetry path with low visibility.

The optical elements in the situations above have been assumed to be placed concentrically about the longitudinal (z) axis. Under such circumstances, a single aperture before the beam splitter yields the same transfer function as two identical apertures placed in each arm after the beam splitter, as shown in Fig. (12). However, the quantum-interference pattern is also sensitive to a relative shift of the apertures in the transverse plane. To account for this, one must include an additional factor in eq. (26)

This extra factor provides yet another degree of control on the quantum-interference pattern for a given aperture form.

As in the case of the shifted ring aperture, visibility becomes negative for certain values of the relative optical-path delay (□), and the interference pattern displays a peak rather than a triangular dip, as shown in Fig. (12 b), something of significant practical value. One can thus use one physical parameter to affect a change in the interference pattern associated with another parameter. In this example, observations made at the center of the interference pattern show what would be a polarization destructive interference minimum become an polarization interference maximum, when a spatial parameter (wave-vector) is altered.

The interference patterns generated in this work are seen to be influenced by the profiles of the apertures in the optical system, which admit wave vectors in specified directions. Including a finite bandwidth for the pump field strengthens this dependence on the aperture profiles, clarifying why the asymmetry was first observed in the ultrafast regime.

The multi-parameter entangled nature of the two-photon state generated by SPDC allows transverse spatial effects to play a role in polarization-based quantum-interference experiments. In contrast to the usual single-direction polarization entangled state, the wide-angle polarization-entangled state offers a richness that can be exploited in a variety of applications.

4. Conclusion

we have developed adescription of two-photon type – II spontanouse parametric down conversion produced when ultra short pulse from afemtosecond laser are

used to pump a non-linear medium , as well as the associated two photon interference effect . in view of the presented results, the following conclusions have been drawn.

Asymmetric interference dip are the order of the short crystal ;however ,distinct and unusual asymmetries emerge in the dips when long crystal are used . The profiles of the aperture used in the optical system have a large effect on The interference pattern .

The coincidence visibility decreases dramatically with increasing crystal length when using pulsed pump , reversing the state when used CW pump a specially with small aperture diameter, the visibility decrease slowly. The effect of the pump beam diameter on the quantum interference pattern is shown to be negligible for a typical range of pump diameter values used.

5. References

[1] N. Gisin, G. Ribordy, W. Tittel, and H. Zbinden, "Quantum cryptography', Reviews of Modern Physics, Vol. 74, January(2002).

[2] A. F. Abouraddy, K. C. Toussanit, A. V.Sergienco, B. E. Salah, and M. C. Teich, "Entangled photon ellipsometry" J.Opt.Soc.Am.B/ vol. 19, No.4, (2002).

[3] E. Forestieri, " Optical Communication Theory and Techniques", Springer Science and Business Media, Inc.(2005).

[4] D. Ljunggren, " Entanglement in quantum communication ", Ph.D. Thesis, Stockholm, Sweden, (2006).

[5] M. Duˇsek, and K. Br´adler,"The effect of multi-pair signal states in quantum cryptography with entangled photons" arXiv:quant-ph/0011007v1July 7, (2007)

[6] G. Di Giuseppe, L. Haiberger, and F. De Martini, "Quantum interference and in distinguishability with femtosecond pulses", Phys. Rev. A, Vol.56, No. 1, (1997).

[7] A.V.Sergienco, M. Atatuse, Z. Walton, G.Jaeger,"Quantum Cryptography using femtosecond pulsed parametric down conversion" , Phy. Rev. A, Vol.60, No. 4,(1999).

[8] M. Atature, G. D. Giuseppe, M. shaw, Alexander V. Sergienko, B. E.A. Saleh, and M. G. Teich, "Multiparameter Entanglement in Femtosecond Parametric Down Conversion", Phys.Rev., A, Vol.65, No.6,(2002).

[9] M. Atature, A. V. Sergienko, B. M. Jost, B. E.A. Saleh, and M. C. Teich, "Partial Distinguishability in Femtosecond Optical Spontanouse Parametric Down Conversion", Phys.Rev. Lett, Vol.83, No. 7,(1999) .

[10] A. V. Sergienko, G. S. Jaeger, G. Di Giuseppe, B. E. A. Saleh, " Quantum Information Processing and Precise Optical Measurement with Hyper Entangled Quantum State", Quantum Imaging Laboratory, Department of Electrical and Computer Engineering (2002).

[11] J.C.Diels & W.Rudolph, "Ultrashort laser pulse phenomena", Academic press, San Diego, (1996).

[12] Y. Ho Kim, M. V. Chekhova, S. P. kulik, M. H. Rubin, and Y. Shih,, " Interferometric Bell State Preparation Using Femtosecond pulse Pump", Phys.Rev., A, Vol.63, No.6,(2001).

[13] J. J. Perina, A. V. sergienko, B. M. Jost, B. E.A. Saleh, and M. C. Teich, "Dispersion in femtosecond Entangled Two-Photon Interference", Phys.Rev., A, Vol.59, No. 3,(1999).

[14] M. Hendrych, "Experimental Quantum Cryptography", Ph.D. Thesis, department of optics, Palacky University, Olomouc, (2002).

الخلاصة

تعد السرية العالية هي الهدف الرئيسي في مجال التشفير الكمي التي يمكن الحصول عليها بأعتماد مصادر الفوتونات المفردة، لدا فقد تمت دراسة مصادر الفوتونات المتشابكة وبيان كيفية تأثير العناصر البصرية لمنظومات التشفير الكمي على معدل حساب التزامن وقابلية الرؤيا.

كرست التحليلات النظرية في هده الاطروحة لدراسة نمط التداخل لسعة الفوتونات الثنائية والمولدة بطريقة SPDC (Spontaneous Parametric Down Conversion) في البلورات اللاخطية (BBO) والتي يتم ضخها بأعتماد نبضات ضوئية قصيرة جدا. درست قابلية الرؤيا كدالة لتأخير المسار البصري ولعدة معلمات مثل طول البلورة، وشكل وحجم الفتحة.

يمكن السيطرة على شكل نمط التداخل بأستخدام فتحات دات اشكال واحجام مختلفة، ففي حالة الضخ المستمر واستخدام فتحة دائرية ، فان اعلى قابلية الرؤيا واكثرها تماثلا يحدث عند قطر فتحة منخفض (b=0.5mm) وعند الاقطار الكبيرة فان نمط التداخل يكون اكثر اتساعا واقل تماثلاو اما في حالة الضخ النبضي، فنحصل على تداخل غيرمتماثل وهدا يزداد مع زيادة قطر البلورة ونقصان قطر الفتحة. بينما يتم الحصول على التماثل في نمط التداخل عند استخدام فتحة افقية وبابعاد (1x7mm).

ان جميع نتائج هدا العمل استخلصت بأستخدام تقنيات رقمية ، واتي تم بها بناء برامج الحل المختلفة. فمثلا استخدمت طريقة (Adaptive Simpson Quaderator) للحل الرقمي في التكاملات المزدوجة(double integral) لبعض المعادلات ، بينما استخدمت طريقة (Adaptive Lobatto Quaderator Method) للحل الرقمي للتكامل المفرد، والطريقة الاخيرة تكون اكثر كفاءة عندما يراد التعامل مع دقة عالية ونعومة تكامل.

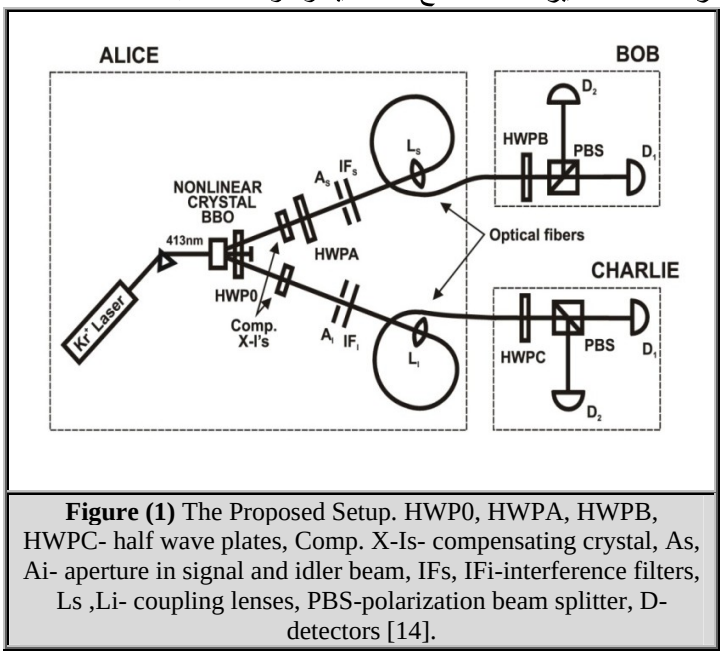

Figure (1) The Proposed Setup. HWP0, HWPA, HWPB, HWPC- half wave plates, Comp. X-Is- compensating crystal, As, Ai- aperture in signal and idler beam, IFs, IFi-interference filters, Ls ,Li- coupling lenses, PBS-polarization beam splitter, D-detectors [14].

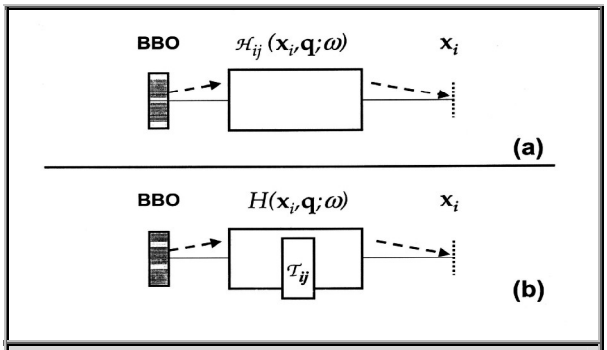

Figure (2) (a) Illustration of the idealized setup for observation of quantum interference using SPDC, (b) Transfer function can be factorized into diffraction dependent and independent component [10].

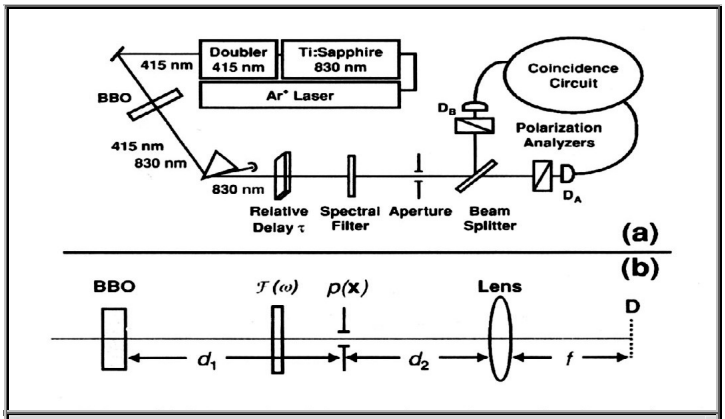

Figure (3) (a) Schematic of the experimental setup for observation of quantum interference using type-II collinear SPDC. (b) The path from the crystal output plane to the detector input plane. F(ω) represents an (optional) filter transmission function, p(x) is an aperture function, and f is the focal length of the lens.[10]

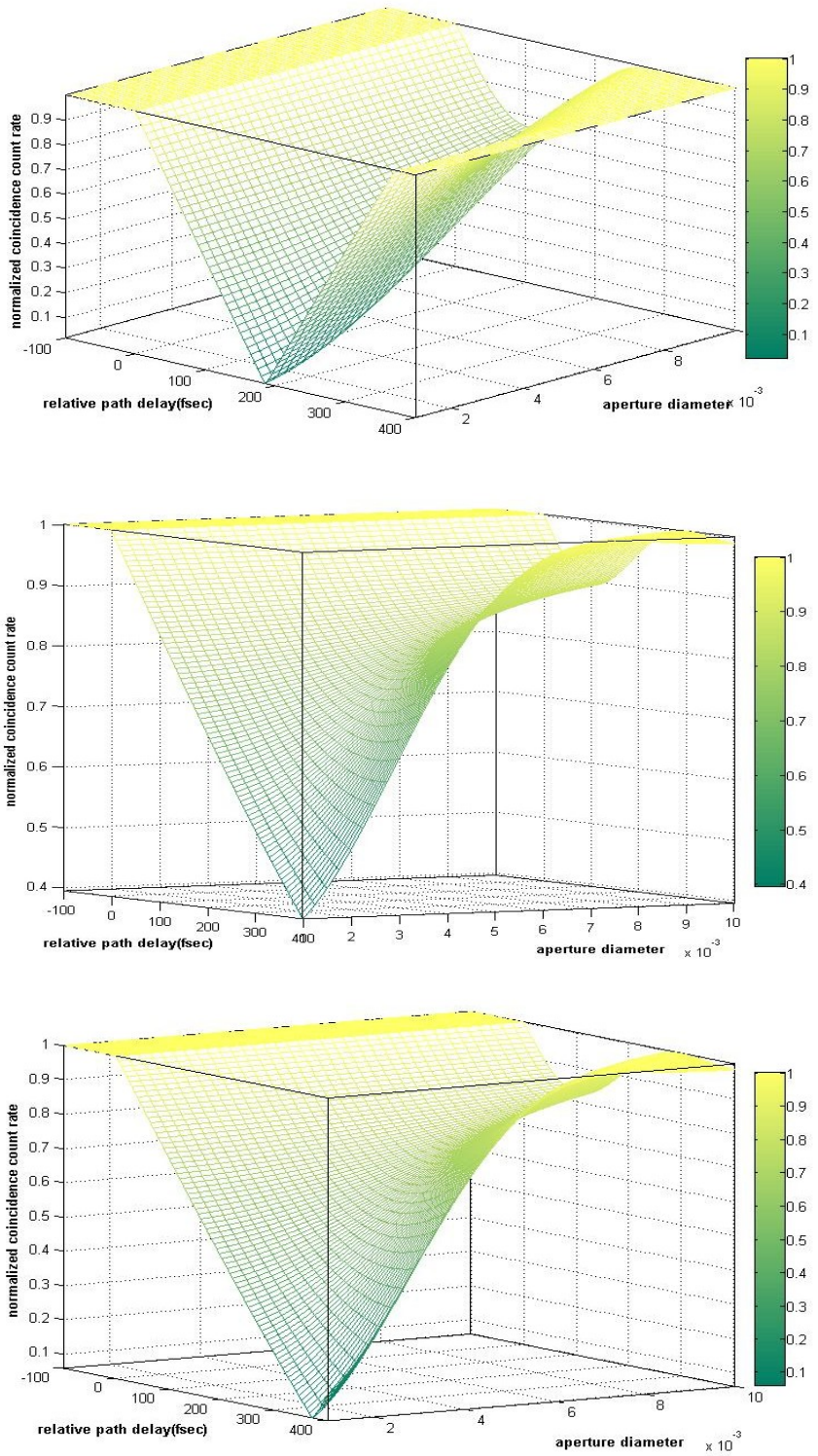

Figure (4) Coincident count rate as a function of optical path delay for different aperture diameter (b).for various crystal length(a- L=1.5, b- L=3, c- L= 5mm).

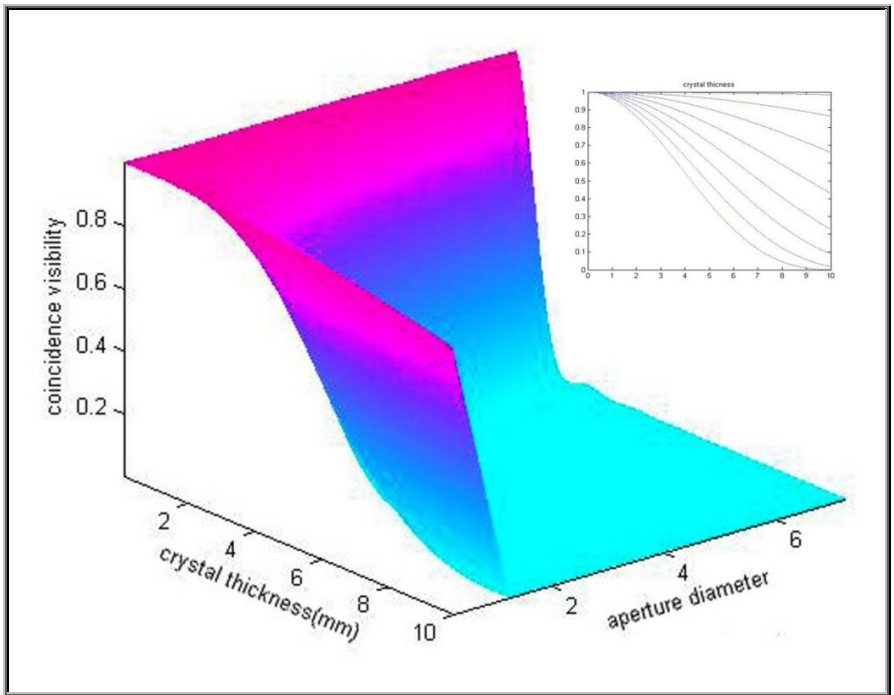

Figure (5) Coincident visibility as a function of crystal thickness for different circular aperture diameter for CW SPDC.

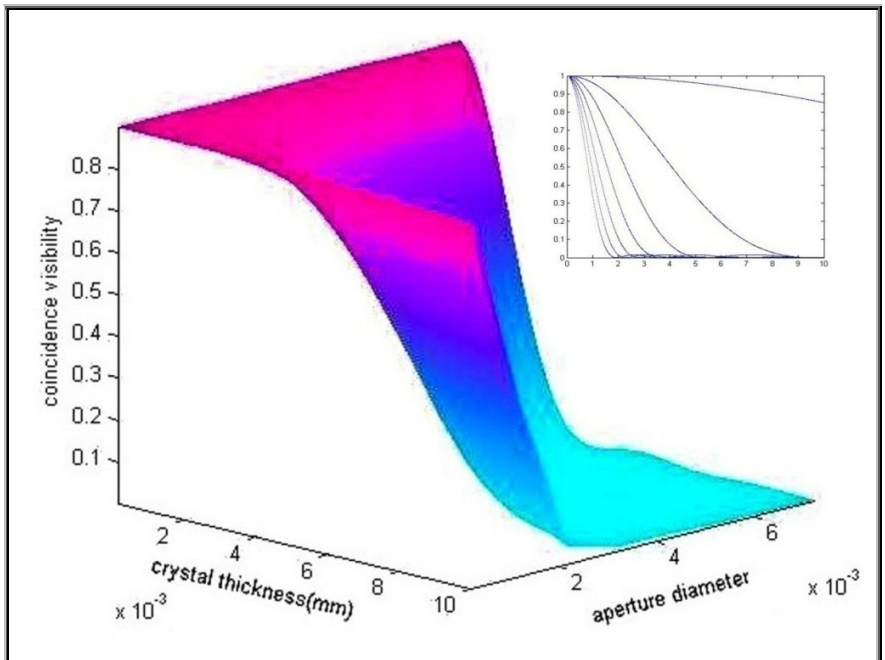

Figure (6) coincident visibility as a function of crystal thickness for various circular aperture diameter for pulsed SPDC.

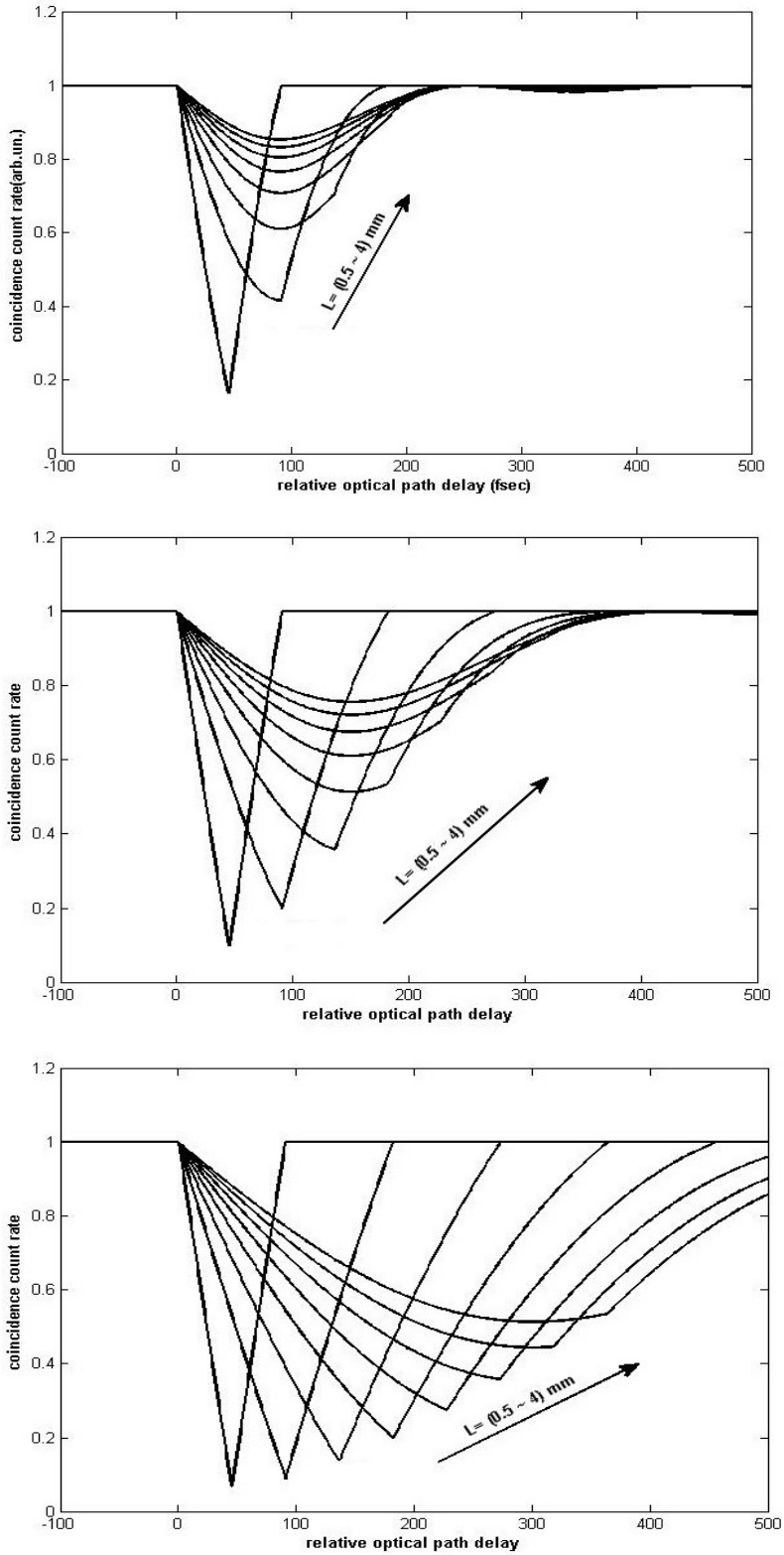

Figure (7) Normalized coincident count rate as a function of relative optical path delay for different values of aperture diameter a-(b=2.5), b- (b=5mm), c- (b=10mm).

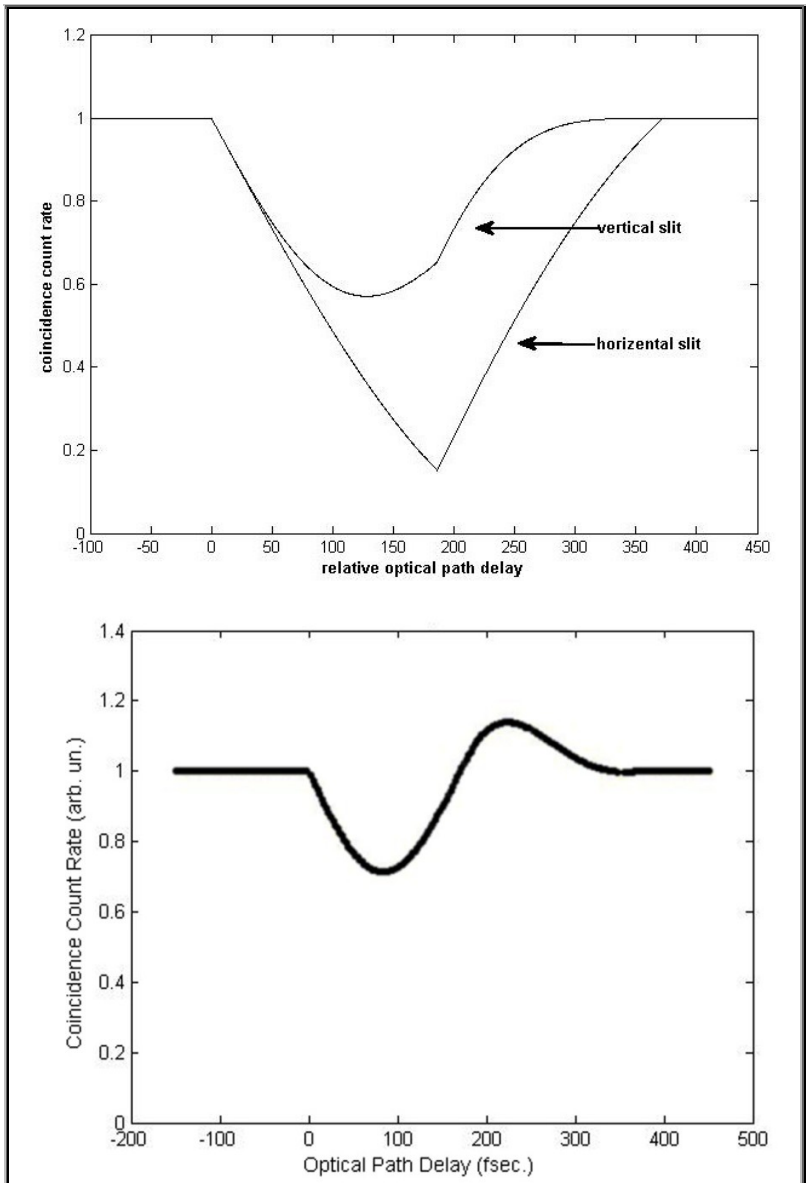

Figure (8) The normalized coincidence rate for a CW pimp 1.5 mm BBo in the presence of avert iced slit aperture with a =7 mm and b=1mm.

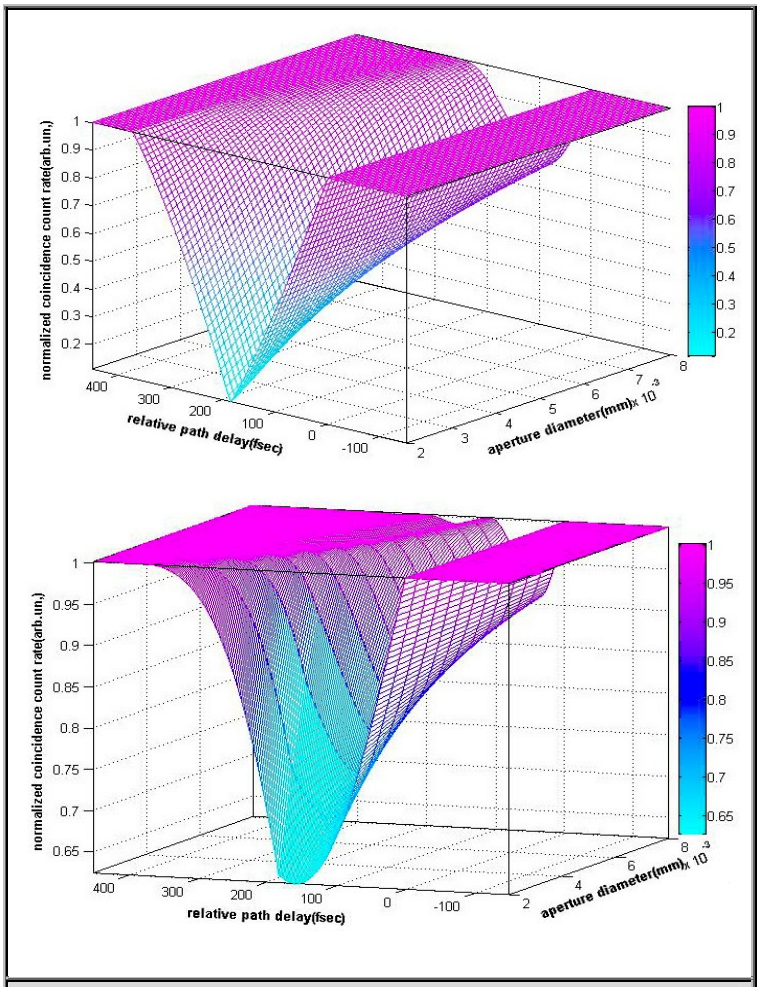

Figure (9) coincident count rate versus optical path delay with rotation 45 of slit aperture.

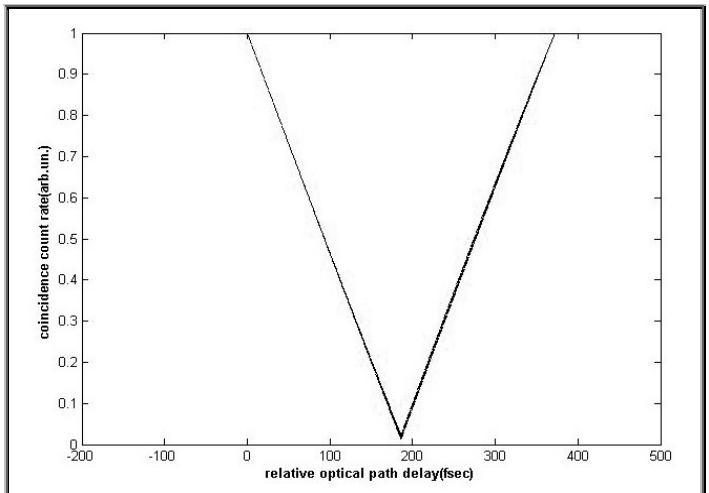

Figure (10) normalized coincident count as a function of relative optical path delay for different circular aperture diameter (b) for(a-CW pump, b- pulse pump).

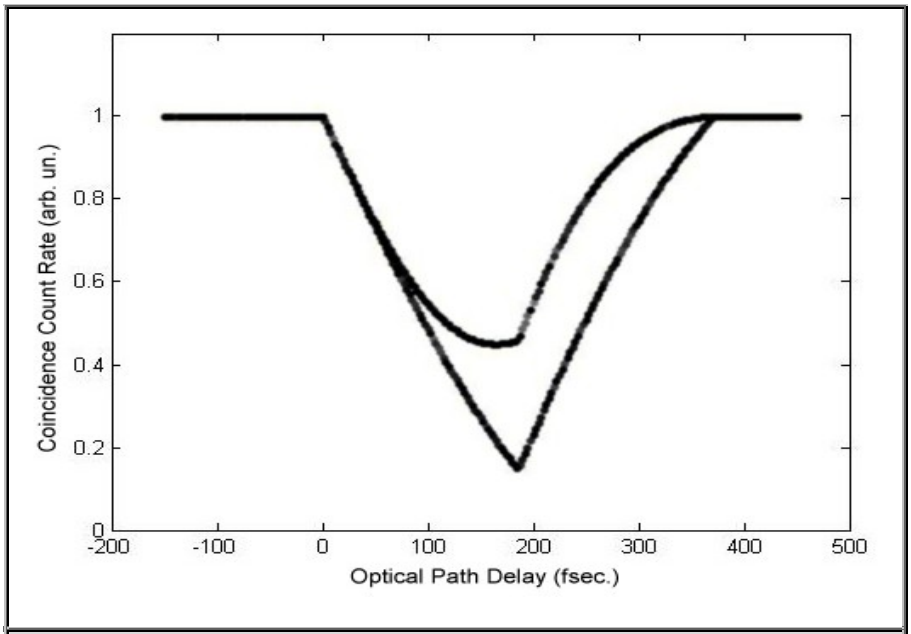

Figure (11) coincident count as a function of relative optical path delay for different pump beam diameter(b_p = (0.5. 1.5, 5)mm).

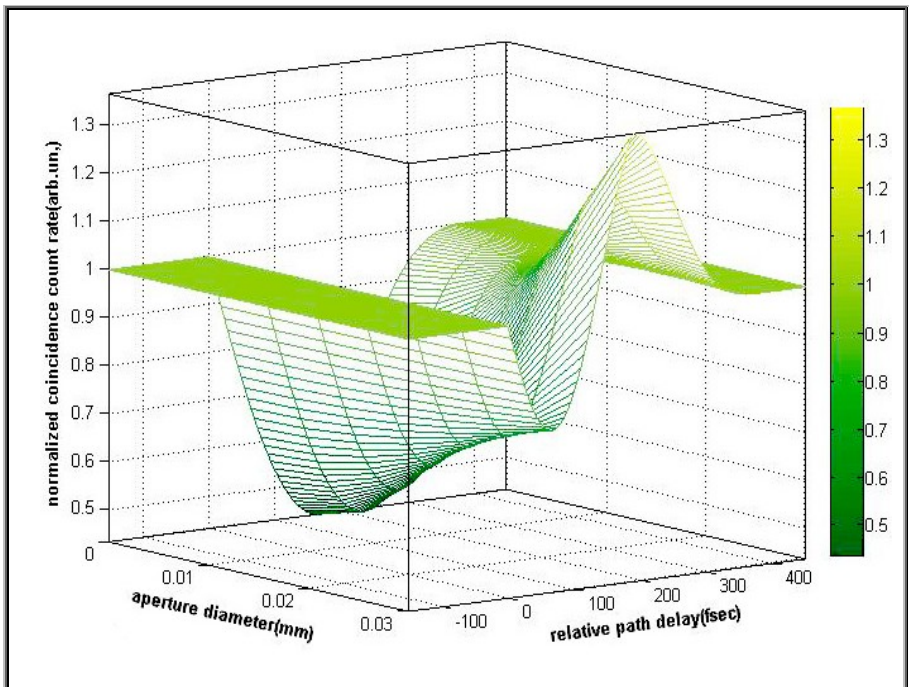

Figure (12) coincident count as a function of relative optical path delay for a-shifted slit aperture , b-shifted ring aperture.